Flavour anomalies and the muon $g-2$ from feebly interacting particles

Luc Darmé,[1,*] Marco Fedele,[2,†] Kamila Kowalska,[3,‡] and Enrico Maria Sessolo[3,§]

[1] *INFN, Laboratori Nazionali di Frascati, C.P. 13, 100044 Frascati, Italy*
[2] *Institut für Theoretische Teilchenphysik, Karlsruhe Institute of Technology, D-76131 Karlsruhe, Germany*
[3] *National Centre for Nuclear Research, ul. Pasteura 7, 02-093 Warsaw, Poland*

We perform a phenomenological analysis of simplified models of light, feebly interacting particles (FIPs) that can provide a combined explanation of the anomalies in $b \to s l^+ l^-$ transitions at LHCb and the anomalous magnetic moment of the muon. Different scenarios are categorised according to the explicit momentum dependence of the FIP coupling to the $b-s$ and $\mu-\mu$ vector currents and they are subject to several constraints from flavour and precision physics. We show that a phenomenologically viable combined solution to the muon $g-2$ and flavour anomalies always exists if a vector with mass larger than 4 GeV is exchanged. Interestingly, the LHC has the potential to probe this region of the parameter space by increasing the precision of the $Z \to 4\mu$ cross-section measurement. Conversely, we find that solutions based on the exchange of a lighter vector, in the $m_V < 1\,\text{GeV}$ range, are essentially excluded by a combination of $B \to K +$ invisible and W-decay precision bounds.

I. INTRODUCTION

Feebly interacting particles (FIPs) represent a very large and well-motivated category of new physics (NP) scenarios. Loosely defined as new light particles with mass below the electroweak symmetry-breaking (EWSB) scale and with a feeble interaction with Standard Model (SM) fields, FIPs encompass NP particles as diverse as the dark photon and axion-like particles. A particularly exciting possibility [1–8] is that one or more FIPs may be responsible for the anomalies in lepton-flavour universality violating (LFUV) observables recently confirmed in new data from LHCb and for the discrepancy between the measured value of the anomalous magnetic moment of the muon and its SM expectation.

The LHCb Collaboration recently released an updated measurement of the ratio $R_K = \text{BR}(B \to K\mu^+\mu^-)/\text{BR}(B \to Ke^+e^-)$, which included the full Run I + Run II data sets. The current value deviates from the SM prediction by more than $3\,\sigma$ [9]. Once the LFUV ratio $R_{K^*} = \text{BR}(B \to K^*\mu^+\mu^-)/\text{BR}(B \to K^*e^+e^-)$ [10, 11] and the branching ratios and angular analyses of other decays mediated by $b \to s\, l^+ l^-$ transitions [12–21] are considered as well, a global picture emerges, pointing to the potential presence of NP interacting with the muons. These contributions are statistically favoured compared to the SM prediction alone, at the level of more than $5\,\sigma$ [22–33].

Equally intriguing is the recent measurement of the anomalous magnetic moment of the muon by the E989 experiment at Fermilab [34]. The experimental collaboration reports a $3.3\,\sigma$ deviation from the value expected in the SM [35–54]. When the new measurement is statistically combined with the previous experimental determination, obtained a couple of decades ago at Brookhaven [55], one obtains [34]

$$\delta(g-2)_\mu = (2.51 \pm 0.59) \times 10^{-9}\,, \tag{1}$$

which yields a deviation from the SM data-driven prediction at the $4.2\,\sigma$ level.

If the LFUV anomalies and $\delta(g-2)_\mu$ are due to the interactions of one or more FIPs in the MeV to GeV range, one expects the accompanying presence of new flavoured physics around the TeV scale (see, e.g., Ref. [8]). On the one hand, higher-dimensional FIP interactions, such as the ones characteristic of axion-like particle models, are simply effective field theories (EFTs) requiring an ultraviolet (UV) completion. On the other hand, even for renormalisable FIP interactions the presence of NP at the EWSB scale is often required, for instance to evade the strong bounds from neutrino trident production, which otherwise drastically constrains a solution to the $(g-2)_\mu$ anomaly based on light states [56].

While for generic processes occurring at scales much lower than the EWSB scale a model-independent description of NP effects via the Weak Effective Theory (WET) has proved invaluable in describing flavour-violating meson decay, the WET fails to account properly for the possibility of one ore more extra light, but hidden, degrees of freedom, as it is not by construction equipped to take into account the effects of momentum-dependent couplings, or the presence of possible resonances in the experimental energy bins. We thus consider in this work EFT operators more adapt to the study of $b \to s$ and μ-related physics in the presence of FIPs [57, 58] (see e.g. the dark-matter motivated constructions, for instance Refs. [59–63]).

To this end, we construct operators that parametrise the interactions of a FIP with Lorentz-invariant vector bilinears of the $b-s$ and $\mu-\mu$ current, in agreement with the measurement of the LFUV and $(g-2)_\mu$ anomalies. They are characterised by increasing powers of the FIP momentum transferred in the low-energy process. We

* luc.darme@lnf.infn.it
† marco.fedele@kit.edu
‡ kamila.kowalska@ncbj.gov.pl
§ enrico.sessolo@ncbj.gov.pl

then perform a comprehensive analysis of the constraints that can be applied on the Wilson coefficients of these new operators. Constraints arise from several sources: direct measurements of the branching ratios for $B \to K +$ invisible and $B \to K^* \mu^+ \mu^-$ resonant decays, the measurements of BR($B_s \to \mu^+ \mu^-$) and B_s-mixing, and several precision measurements associated with the W and Z boson decay widths. The aim is that of providing a concise but broad model-independent picture of the current phenomenological status of a light-FIP solution to the muon anomalies.

The paper is organised as follows. In Sec. II we introduce the operators suitable to describing FIP interactions with LFUV processes. In Sec. III we provide the matching to the WET basis usually employed in analyses of rare meson decays. The list of applied constraints is introduced in Sec. IV. The result of a global scan in the new operator basis are presented and discussed in Sec. V, and we conclude in Sec. VI.

II. EFT PLUS LIGHT DEGREES OF FREEDOM

We introduce in this section Dark EFT (DEFT) operators connecting a generic FIP to the (axial-)vector SM currents relevant for the LFUV and $(g-2)_\mu$ anomalies.

a. Spin-1 FIP We parametrise the exchange of a light vector V out of the left-handed $b-s$ current, in agreement with the results of the global fits, in terms of the following operators [5]:[1]

$$\mathcal{Q}_4^{bsV} = (\bar{s}\gamma_\rho P_L b)\, V^\rho \,, \tag{2}$$

$$\mathcal{Q}_6^{bsV} = (\bar{s}\gamma_\rho P_L b)\, \partial_\sigma V^{\rho\sigma} \,, \tag{3}$$

where we have used the field strength tensor $V^{\rho\sigma} = \partial^\rho V^\sigma - \partial^\sigma V^\rho$. We complete Eqs. (2), (3) with the corresponding interactions with the muon current,

$$\mathcal{Q}_4^{\mu\mu V} = (\bar{\mu}\gamma_\rho \mu)\, V^\rho \,, \qquad \widetilde{\mathcal{Q}}_4^{\mu\mu V} = \left(\bar{\mu}\gamma_\rho\gamma^5\mu\right) V^\rho \,, \tag{4}$$

$$\mathcal{Q}_6^{\mu\mu V} = (\bar{\mu}\gamma_\rho \mu)\, \partial_\sigma V^{\rho\sigma} \,, \quad \widetilde{\mathcal{Q}}_6^{\mu\mu V} = \left(\bar{\mu}\gamma_\rho\gamma^5\mu\right) \partial_\sigma V^{\rho\sigma} \,. \tag{5}$$

Since we do not specify the origin of these interactions, Eqs. (2)-(5) will serve in describing the B-physics for all light vector states. These include, in particular, the GeV-scale top-philic particle in Ref. [64] and the renormalisable model introduced in Ref. [8].

b. Spin-0 FIP: the pNGB We consider next the case of a (pseudo-)scalar FIP, a, possibly a pseudo Nambu-Goldstone boson (pNGB). The standard derivative interaction term with the quark current reads

$$\mathcal{Q}_5^{bsa} = \frac{1}{2}\,\partial_\rho a\, (\bar{s}\gamma^\rho P_L b) \,, \tag{6}$$

and

$$\mathcal{Q}_5^{\mu\mu a} = \frac{1}{2}\,\partial_\rho a\, (\bar{\mu}\gamma^\rho \mu) \,, \qquad \widetilde{\mathcal{Q}}_5^{\mu\mu a} = \frac{1}{2}\,\partial_\rho a\, \left(\bar{\mu}\gamma^\rho\gamma^5\mu\right) \,, \tag{7}$$

are the corresponding couplings to the muon current. These interactions are strongly constrained by flavour physics and, more importantly for our purposes, do not lead to the vector four-fermion operators $\mathcal{O}_9^{\mu(\prime)}$ and $\mathcal{O}_{10}^{\mu(\prime)}$ of the WET, which induce the solution to the LFUV anomalies preferred in the global scans. We therefore leave the study of these operators for future work.

c. FIPs as dark matter: spin 0, 1/2 When the light state is a stable new particle, which can play the role of dark matter, one needs to include operators with two FIP insertions at dimension 6. Using the dark current,

$$\mathcal{J}_D^\rho = \begin{cases} i\,(S^*\partial^\rho S - S\partial^\rho S^*) & (\text{scalar},\ D=S) \\ \bar{\chi}\gamma^\rho\chi \,, & (\text{fermion},\ D=\chi) \end{cases} \tag{8}$$

we can then define

$$\mathcal{Q}_6^{\mu\mu\chi\chi} = \mathcal{J}_\chi^\rho\, (\bar{\mu}\gamma_\rho\mu) \,, \quad \widetilde{\mathcal{Q}}_6^{\mu\mu\chi\chi} = \mathcal{J}_\chi^\rho\, \left(\bar{\mu}\gamma_\rho\gamma^5\mu\right) \,, \tag{9}$$

and

$$\mathcal{Q}_6^{bs\chi\chi} = \mathcal{J}_\chi^\rho\, (\bar{s}\,\gamma_\rho P_L b) \,, \tag{10}$$

and equivalent operators can be defined in the scalar case, with $\chi \to S$.

These effective interactions can be used to parametrise, for example, UV completions to the WET operators $\mathcal{O}_9^{\mu(\prime)}$, $\mathcal{O}_{10}^{\mu(\prime)}$ based on dark-matter induced box loops, in the case where the dark matter is relatively light. Note, however, that in such a minimal scenario the dark matter mass is expected to be large enough to evade strong limits for the direct decay $B \to K +$ invisible [8].

III. MATCHING WITH THE WET

In order to quantify the effect of DEFT operators on flavour observables, we first create a dictionary between the set of DEFT operators and the WET. The procedure gives to an explicit momentum dependence of the WET operators, of the type explored, e.g., in Refs. [1, 4, 6, 8].

A. Tree-level matching

a. Spin-0 FIP The critical ingredient in matching both theories is that we are interested in physical processes in which the muons are on-shell. Given two on-shell external muons of four-momenta k_1, k_2, emerging from the exchange of a FIP of momentum $q = k_1 + k_2$, the equations of motions yield

$$q^\rho\, (\bar{\mu}\gamma_\rho\mu) = 0 \tag{11}$$

$$q^\rho\, \left(\bar{\mu}\gamma_\rho\gamma^5\mu\right) = 2M_\mu\, \left(\bar{\mu}\gamma^5\mu\right) . \tag{12}$$

[1] We leave for future work the dimension 5 case, as it couples the FIP to the tensor SM current and leads to a starkly different phenomenology.

A direct consequence of the above equations is that the derivative scalar current introduced in Eqs. (6) and (7) will be matched to the standard pseudoscalar interactions $\mathcal{O}_P^{\mu(\prime)}$, and thus cannot generate the WET vector operators $\mathcal{O}_9^{\mu(\prime)}$ and $\mathcal{O}_{10}^{\mu(\prime)}$.

By repeating the argument for "on-shell" initial quarks with $q = p_b - p_s$, one obtains

$$(\bar{s}\gamma_\rho P_L b)\, q^\rho = M_s\,(\bar{s}P_L b) - M_b\,(\bar{s}P_R b)\,. \tag{13}$$

The above equality is useful for deriving several of the matching conditions in the remainder of this section.

b. Spin-1 FIP We write the vector FIP propagator in the form

$$\Pi^{\rho\sigma} = \frac{-i\left(g^{\rho\sigma} - q^\rho q^\sigma/m_V^2\right)}{\Pi}\,, \qquad \text{with} \quad \Pi = q^2 - m_V^2 + i\Gamma_V m_V\,, \tag{14}$$

where m_V and Γ_V indicate, respectively, the mass and total decay width of the light NP vector V^ρ.

By considering the $b \to s\mu\mu$ process via a vector FIP exchange, we can construct a matching table between the DEFT and the WET. Let us derive, for example, the matching to the WET of an interaction involving operators $\mathcal{Q}_6^{bsV}$ and $\widetilde{\mathcal{Q}}_4^{\mu\mu V}$ in Eqs. (3) and (4). One finds

$$\begin{aligned}\mathcal{H}_{\text{eff}} &= -i\,\widetilde{\mathcal{C}}_4^{\mu\mu V}\mathcal{C}_6^{bsV}/\Lambda^2\,(\bar{s}\gamma_\rho P_L b)\left(q^2 g^{\sigma\rho} - q^\sigma q^\rho\right) \\ &\qquad \times \Pi_{\sigma\nu}\left(\bar{\mu}\gamma^\nu\gamma^5\mu\right) \\ &= -\frac{\widetilde{\mathcal{C}}_4^{\mu\mu V}\mathcal{C}_6^{bsV}/\Lambda^2}{\Pi}\,(\bar{s}\gamma_\rho P_L b)\left(q^2\delta^\rho_\nu - q^\rho q_\nu\right)\left(\bar{\mu}\gamma^\nu\gamma^5\mu\right) \\ &= -\frac{\widetilde{\mathcal{C}}_4^{\mu\mu V}\mathcal{C}_6^{bsV}}{\Lambda^2\,\Pi}\frac{4\pi}{\alpha_{\text{em}}}\left[q^2\mathcal{O}_{10}^\mu + 2M_\mu\left(M_s\mathcal{O}_P^{\mu\prime} - M_b\mathcal{O}_P^\mu\right)\right]\,,\end{aligned} \tag{15}$$

where in the last line we have used Eq. (13). The above relation is expressed in terms of the UV cutoff, Λ, and the DEFT dimensionless coefficients $\mathcal{C}_6^{bsV}$, $\widetilde{\mathcal{C}}_4^{\mu\mu V}$.

Following a similar procedure, we can match to the WET all the operators introduced in Sec. II*a*. The results are presented in Table I.

The WET coefficients C_9^μ and C_{10}^μ, emerging as favoured in global flavour analyses, can be conversely expressed in terms of DEFT coefficients. One gets,

$$C_9^\mu = -\frac{4\pi\mathcal{N}}{\alpha_{\text{em}}}\frac{(\mathcal{C}_4^{bsV} - \frac{q^2}{\Lambda^2}\mathcal{C}_6^{bsV})(\mathcal{C}_4^{\mu\mu V} - \frac{q^2}{\Lambda^2}\mathcal{C}_6^{\mu\mu V})}{q^2 - m_V^2 + i\Gamma_V m_V}\,, \tag{16}$$

$$C_{10}^\mu = -\frac{4\pi\mathcal{N}}{\alpha_{\text{em}}}\frac{(\mathcal{C}_4^{bsV} - \frac{q^2}{\Lambda^2}\mathcal{C}_6^{bsV})(\widetilde{\mathcal{C}}_4^{\mu\mu V} - \frac{q^2}{\Lambda^2}\widetilde{\mathcal{C}}_6^{\mu\mu V})}{q^2 - m_V^2 + i\Gamma_V m_V}\,, \tag{17}$$

where $\mathcal{N}^{-1} = (4G_F/\sqrt{2})\,V_{tb}V_{ts}^*$.

c. An explicit UV example We conclude this subsection by providing an explicit example of the matching between the DEFT operators and a renormalisable UV-complete model in the case of a vector FIP, focusing on the flavour-violating coupling to b and s.

Let us consider the SM extended by a "dark" $\mathrm{U}(1)_D$ gauge group, whose gauge boson is a light V. Let us then introduce a scalar field ϕ and a multiplet χ of vector-like fermions of mass m_χ whose charges with respect to $\mathrm{SU}(3)_c\times\mathrm{SU}(2)_L\times\mathrm{U}(1)_Y\times\mathrm{U}(1)_D$ are given by

$$\phi : (\mathbf{1},\mathbf{1},0,Q_\phi) \qquad \chi : (\mathbf{3},\mathbf{2},1/6,Q_\chi)\,. \tag{18}$$

When $Q_\phi = Q_\chi$ the fields in Eq. (18) admit Yukawa interactions with the SM quark doublets $Q_i = (P_L u_i, P_L d_i)^T$ (of generation $i = 2,3$) of the type

$$\mathcal{L} \supset Y_Q^i\,\phi\bar{\chi}\,Q_i + \text{H.c.} \tag{19}$$

Depending on whether or not the field ϕ acquires a vacuum expectation value (vev) different DEFT operators of the $b-s$ current are generated at the leading order from the coupling in Eq. (19). If ϕ develops a vev, v_ϕ, the effective coupling of V to $b-s$, which is generated via the mixing of the SM and NP quarks, does not carry q^2 dependence and thus gives rise to the operator $\mathcal{Q}_4^{bsV}$. One gets

$$\mathcal{C}_4^{bsV} = g_D Q_\phi \frac{Y_Q^{s*}\,Y_Q^b\,v_\phi^2}{2\,m_\chi^2 + \left(\left|Y_Q^s\right|^2 + \left|Y_Q^b\right|^2\right)v_\phi^2}\,, \tag{20}$$

where g_D is the "dark" gauge coupling. The phenomenology of the light gauge boson V in relation to $R_{K^{(*)}}$ was analysed, e.g., in Ref. [2].

If, on the other hand, the scalar ϕ does not develop a vev and $\mathrm{U}(1)_D$ is broken by other means unspecified here, the coupling of V to the $b-s$ current is generated via a penguin diagram constructed out of a $\phi\chi$ loop. Terms presenting an explicit q^2 dependence give rise to the operator $\mathcal{Q}_6^{bsV}$. Its Wilson coefficient reads

$$\frac{\mathcal{C}_6^{bsV}}{\Lambda^2} = \frac{g_D\,Q_\phi Y_Q^{s*}\,Y_Q^b}{16\pi^2 m_\chi^2}\mathcal{F}\left(\frac{m_\phi^2}{m_\chi^2}\right)\,, \tag{21}$$

where m_ϕ is the mass of the scalar field and the loop function is [65]

$$\mathcal{F}(x) = \frac{3 - 3x + (1+2x)\ln x}{6\,(x-1)^2}\,. \tag{22}$$

When $m_\phi \ll m_\chi \approx \Lambda$, $\mathcal{Q}_6^{bsV}$ becomes the dominant operator emerging from the $\phi\chi$ loop, thanks to the logarithmic enhancement in Eq. (22). The phenomenology of this "split" dark sector was analysed in Ref. [8] and q^2-dependent operators were considered also in Refs. [1, 4, 6].

Analogous to this is the case where fermion and scalar multiplet charges are swapped in Eq. (18) [8], and UV constructions along similar lines can be considered to generate other DEFT operators, e.g., those involving the muon current in Eqs. (4), (5).

Note that the DEFT coefficients $\mathcal{C}_4^{bsV}$, $\mathcal{C}_6^{bsV}$ – similarly to $C_{9(10)}^\mu$ in the WET – do not run at the leading

	$\mathcal{Q}_4^{bsV}$	$\Lambda^2\mathcal{Q}_6^{bsV}$
$\mathcal{Q}_4^{\mu\mu V}$	$-\mathcal{O}_9^\mu$	$q^2\mathcal{O}_9^\mu$
$\widetilde{\mathcal{Q}}_4^{\mu\mu V}$	$-\left(\mathcal{O}_{10}^\mu + \frac{2M_\mu\left(-M_b\mathcal{O}_P^\mu + M_s\mathcal{O}_P^{\mu\prime}\right)}{m_V^2}\right)$	$q^2\left(\mathcal{O}_{10}^\mu + \frac{2M_\mu\left(-M_b\mathcal{O}_P^\mu + M_s\mathcal{O}_P^{\mu\prime}\right)}{q^2}\right)$
$\Lambda^2\mathcal{Q}_6^{\mu\mu V}$	$q^2\mathcal{O}_9^\mu$	$-q^4\mathcal{O}_9^\mu$
$\Lambda^2\widetilde{\mathcal{Q}}_6^{\mu\mu V}$	$q^2\left(\mathcal{O}_{10}^\mu + \frac{2M_\mu\left(-M_b\mathcal{O}_P^\mu + M_s\mathcal{O}_P^{\mu\prime}\right)}{q^2}\right)$	$-q^4\left(\mathcal{O}_{10}^\mu + \frac{2M_\mu\left(-M_b\mathcal{O}_P^\mu + M_s\mathcal{O}_P^{\mu\prime}\right)}{q^2}\right)$

TABLE I. Matching relations between the DEFT operators relevant for $B \to K^{(*)}\mu^+\mu^-$ physics and the standard WET operators. All products of DEFT coefficients should be multiplied by $4\pi\mathcal{N}/\alpha_{\rm em}/\Pi$. The scale suppression factors are indicated directly in the labels.

order in QCD, since their colour part is simply a vector current [66].[2]

B. Loop-level matching

In the case of FIPs as a dark matter particle one typically obtains the Wilson coefficients of the WET from "candy" diagrams constructed out of the operators in Eqs. (9), (10). By making use of a simple cut-off regularisation, one can derive at one loop the Wilson coefficient C_9^μ from a fermion FIP insertion,

$$C_9^{\mu(\text{ferm.})} = -\frac{\mathcal{N}\,\mathcal{C}_6^{bs\chi\chi}\mathcal{C}_6^{\mu\mu\chi\chi}}{2\,\pi\,\alpha_{\rm em}\,\Lambda^2}\,. \tag{23}$$

A scalar FIP leads to

$$C_9^{\mu(\text{scal.})} = -\frac{\mathcal{N}\,\mathcal{C}_6^{bsSS}\mathcal{C}_6^{\mu\mu SS}}{16\,\pi\,\alpha_{\rm em}\,\Lambda^2}\,. \tag{24}$$

Note that the only scale that enters directly the WET coefficients in Eqs. (23), (24) is the Λ^2 suppression. Their exact value will thus depend on the specific nature of the heavy UV completion and, as a direct consequence, the dark matter mass will have no impact on the flavour anomalies as long as its couplings to the $b-s$ and $\mu-\mu$ current are mediated by states that can be integrated out of the low-energy theory.

IV. FLAVOUR PHYSICS CONSTRAINTS

Global scans combining the constraints from the LFUV ratios R_K and R_{K^*} with the full set of $b \to s l^+ l^-$ branching ratios and angular observables convincingly show the emergence of NP effects in the WET Wilson coefficient C_9^μ, which can be taken alone or in combinations with others. When parametrising the global fit with one NP degree of freedom, the expected size of the Wilson coefficient is $-1.1 \lesssim C_9^\mu \lesssim -0.5$ at $2\,\sigma$ in the single-operator case, or $-0.6 \lesssim C_9^\mu = -C_{10}^\mu \lesssim -0.3$ in a linear combination of $\mathcal{O}_9^\mu$ and $\mathcal{O}_{10}^\mu$ [22–33].

As we have shown in Sec. III A, the insertion of a spin-0 FIP cannot generate the WET operator $\mathcal{O}_9^\mu$ (or $\mathcal{O}_{10}^\mu$). At the same time, Eqs. (23), (24) show that the numerical value of C_9^μ is quite insensitive to the presence of light dark matter-like spin-1/2 and/or spin-0 states with dimension 6 interactions. We can thus choose to limit our attention to the only case in which the presence of a light FIP has direct impact on the $b \to s\,l^+l^-$ global fit: the vector FIP.

The constraints on C_9^μ and other WET coefficients derived from the flavour anomalies lead in this case to a typical order-of-magnitude estimate for the DEFT couplings, obtained from a spin-1 FIP exchange in $b \to s\mu\mu$, see Eqs. (16), (17),

$$\mathcal{C}_{4+\delta_1}^{bsV}\mathcal{C}_{4+\delta_2}^{\mu\mu V}\left(\frac{q}{\Lambda}\right)^{\delta_1+\delta_2} \approx 10^{-9}\,, \tag{25}$$

where $4+\delta_{1,2}$ indicates the dimension of the corresponding operator, and q is the typical energy exchange captured in the experimental bin. For example, the biproduct of operators $\mathcal{Q}_6^{bsV} \times \mathcal{Q}_4^{\mu\mu V}$ develops q^2 dependence in the couplings, while this is not the case for a combination of operators of dimension 4.

The presence of a new light vector particle in the spectrum has far reaching consequence for a variety of SM processes. As is discussed in the literature (see, e.g., Refs. [67–69]), at FIP masses far below the typical energy scale E of a given SM process, the phenomenology is dominated by the FIP longitudinal polarisation V_L as $V_\mu \to \partial_\mu V_L/m_V$. While this mode cancels out for dimension-6 interactions like Eqs. (3) and (5), it dominates for the dimension-4 cases, Eqs. (2) and (4), as they do not corresponds to conserved SM fermionic currents. The interactions presented in Eq. (2) and Eq. (4) lead to tree-level flavour violation, weak-isospin violation (since

[2] Conversely, a DEFT coefficient corresponding to a tensor operator of the type $\mathcal{Q}_5^{bsV} = (\bar{s}\sigma_{\rho\sigma}P_R b)\,V^{\rho\sigma}$, which can also be generated at the loop level by the UV completion, has to be renormalised before being confronted with the low-energy constraints. We leave the treatment of this and other less straightforward cases to future work.

no coupling to neutrinos where included) and an axial-coupling interaction to the SM fermions. We examine in this section the most relevant of the corresponding limits.

A. B-meson constraints

We first consider the constraints related to the many observables focusing on B-meson physics.

a. $B_s \to \mu\mu$ Based on a physical process related to the one generating $B \to K^{(*)}\mu^+\mu^-$ transitions, $\mathrm{BR}(B_s \to \mu^+\mu^-)$ can provide a strong constraint on axial muon interactions. After performing a statistical combination of the full LHCb Run 2 data with the global average of Ref. [70], Ref. [31] finds

$$\mathrm{BR}(B_s \to \mu^+\mu^-)_{\text{exp. ave.}} = (2.93 \pm 0.35) \times 10^{-9} \,. \quad (26)$$

The impact of this constraint on the parameter space differs for the different biproducts of DEFT operators providing a solution to the flavour anomalies. The matching between the WET and DEFT operators relevant for $B_s \to \mu\mu$ decay can be derived from Table I by simply exchanging M_s and M_b.

Referring to the table, a vector FIP exchange via the product $\mathcal{Q}_4^{bsV} \times \widetilde{\mathcal{Q}}_4^{\mu\mu V}$ will generate, besides $\mathcal{O}_{10}^{\mu}$, the WET pseudoscalar operators $\mathcal{O}_P^{\mu}$, $\mathcal{O}_P^{\mu\prime}$. The ratio R_{B_s} between Eq. (26) and the SM prediction, $\mathrm{BR}(B_s \to \mu^+\mu^-)_{\text{SM}} = (3.67 \pm 0.15) \times 10^{-9}$ [71], can be parametrised in this case as

$$\begin{aligned} R_{B_s} &= \frac{\mathrm{BR}(B_s \to \mu^+\mu^-)_{\text{exp.}}}{\mathrm{BR}(B_s \to \mu^+\mu^-)_{\text{SM}}} - 1 \\ &\simeq \frac{8\pi\mathcal{N}\,\mathcal{C}_4^{bsV}\widetilde{\mathcal{C}}_4^{\mu\mu V}}{\alpha_{\text{em}} C_{10}^{\text{SM}}\, m_V^2} \frac{(m_V^2 - M_{B_s}^2)^2}{(m_V^2 - M_{B_s}^2)^2 + m_V^2\Gamma_V^2} \,, \end{aligned} \quad (27)$$

where $C_{10}^{\text{SM}} = -4.31$ and we have taken the small coupling limit. This measurement excludes the SM prediction at 2σ, we thus choose to implement it at $3\,\sigma$ to avoid cutting out all the points with a zero or extremely small contribution. On the other hand, we observe that Eq. (27) is negative if $\mathcal{C}_4^{bsV}\widetilde{\mathcal{C}}_4^{\mu\mu V} < 0$, which implies that NP contributions can potentially bring R_{B_s} closer to the measured value. As we shall see in the next section, this sign choice is indeed preferred for m_V larger than a few GeV. On the other hand, in the low mass regime, $m_V \lesssim 1\,\text{GeV}$, the above result gives at 3σ a strong upper bound,

$$\left|\mathcal{C}_4^{bsV}\widetilde{\mathcal{C}}_4^{\mu\mu V}\right| \lesssim 1.5 \cdot 10^{-10} \left(\frac{m_V}{1\,\text{GeV}}\right)^2 . \quad (28)$$

Conversely, selecting the product $\mathcal{Q}_6^{bsV} \times \widetilde{\mathcal{Q}}_4^{\mu\mu V}$ we find that the NP contribution to $B_s \to \mu\mu$ vanishes exactly, $R_{B_s} = 0$, since the NP term contributing to the axial component is exactly cancelled by the one feeding into the pseudoscalar current. Interestingly, this implies that increasing the sensitivity of the measurement of $\mathrm{BR}(B_s \to \mu^+\mu^-)$ may provide a handle to distinguish scenarios characterised by operators of different dimension.

$\mathcal{Q}_4^{bsV} \times \mathcal{Q}_4^{bsV}$	$-\mathcal{O}_1 + \frac{M_b^2\mathcal{O}_2 + M_s^2\tilde{\mathcal{O}}_2 - 2M_sM_b\mathcal{O}_4}{m_V^2}$
$\Lambda^2\mathcal{Q}_6^{bsV} \times \mathcal{Q}_4^{bsV}$	$-q^2\left(-\mathcal{O}_1 + \frac{M_b^2\mathcal{O}_2 + M_s^2\tilde{\mathcal{O}}_2 - 2M_sM_b\mathcal{O}_4}{q^2}\right)$
$\Lambda^4\mathcal{Q}_6^{bsV} \times \mathcal{Q}_6^{bsV}$	$q^4\left(-\mathcal{O}_1 + \frac{M_b^2\mathcal{O}_2 + M_s^2\tilde{\mathcal{O}}_2 - 2M_sM_b\mathcal{O}_4}{q^2}\right)$

TABLE II. Matching relations between the DEFT and the standard WET operators relevant for B_s-mixing. All products of DEFT coefficients should be multiplied by Π^{-1}. The scale suppression factors are indicated directly in the labels.

b. B_s-mixing $B_s - \bar{B}_s$ transitions can constrain the DEFT operators introduced in Sec. II. We use [72]

$$R_{\Delta M_s} = \frac{\Delta M_s^{\text{exp.}}}{\Delta M_s^{\text{SM}}} - 1 = -0.09 \pm 0.08 \quad (29)$$

to impose a bound on the WET Wilson coefficients of the $b - s$ current as described, e.g., in Ref. [65].

Similarly to the $B_s \to \mu\mu$ case, the severity of the bound strongly depends on which DEFT operator is generated in the UV completion yielding the $b - s$ coupling. We can construct a matching table between the DEFT and the WET operators relevant to this observable. The results are presented in Table II.

Referring to the table, the operator $\mathcal{Q}_4^{bsV}$ gives rise to m_V^2-rescaled $\mathcal{O}_2$, $\widetilde{\mathcal{O}}_2$, and $\mathcal{O}_4$. We obtain, in the small coupling approximation,

$$R_{\Delta M_s} \simeq \frac{(\mathcal{C}_4^{bsV})^2}{C_1^{\text{SM}}(\mu_b)\, m_V^2} \frac{(M_{B_s}^2 - m_V^2)(R_2 M_b^2 - m_V^2)}{(m_V^2 - M_{B_s}^2)^2 + m_V^2\Gamma_V^2} \,, \quad (30)$$

where $C_1^{\text{SM}}(\mu_b) = 7.2 \times 10^{-11}\,\text{GeV}^{-2}$ and $R_2(\mu_b) \simeq -0.9$ is the ratio of the matrix elements $\langle\bar{B}_s|\mathcal{O}_2(\mu_b)|B_s\rangle / \langle\bar{B}_s|\mathcal{O}_1(\mu_b)|B_s\rangle$ (see, e.g., Ref. [73] for an updated value), all computed at the b-quark mass scale, μ_b. As was mentioned above, we have not run the SM Wilson coefficients since we perform the matching directly at the B_s scale. By combining Eq. (30) and Eq. (29) one gets a strong constraint in the $m_V \ll 1\,\text{GeV}$ range: $|\mathcal{C}_4^{bsV}| \lesssim 5 \cdot 10^{-6}\, m_V/\text{GeV}$. Conversely, with UV interactions giving rise to the operator $\mathcal{Q}_6^{bsV}$, Eq. (30) becomes

$$R_{\Delta M_s} = \frac{M_{B_s}^2 (\mathcal{C}_6^{bsV})^2}{\Lambda^4\, C_1^{\text{SM}}(\mu_b)} \frac{(M_{B_s}^2 - m_V^2)(M_{B_s}^2 - R_2 M_b^2)}{(m_V^2 - M_{B_s}^2)^2 + m_V^2\Gamma_V^2} \,, \quad (31)$$

One obtains $|\mathcal{C}_6^{bsV}|\, M_{B_s}^2/\Lambda^2 \lesssim 2 \times 10^{-5}$ in the low m_V region.

c. $B \to K^{(*)}X$ Strong limits arise from the direct measurement of the branching ratios of the V, both in the case of a visible resonance and that of an invisible decay. Resonant decays to visible particles are subject to extremely strong constraints from LHCb in the m_V range between $2M_\mu$ and $M_B - M_{K^*}$ [74]. We apply this bound

following the numerical recasting described in detail in Ref. [8].

To impose bounds on the invisible decay width we use a combination of BaBar results [75, 76].[3] The adopted numerical procedure is described in detail in Appendix A of Ref. [8]. Assuming a large Γ_V to invisible products in the $m_V \ll 1\,\text{GeV}$ range, the bin-dependent bounds on $\text{BR}(B \to K + \text{inv.})$ induce a strong constraint on the coupling to the hadronic current. In the dimension 4 case we get $|\mathcal{C}_4^{bsV}| \lesssim 10^{-8}\, m_V/\text{GeV}$, whereas for the operator of dimension 6 we get $|\mathcal{C}_6^{bsV}/\Lambda^2| \lesssim 5 \cdot 10^{-9}\,\text{GeV}^{-2}$.

B. Lepton sector constraints

The second set of constraints relies instead on probing the FIP interactions with muons, the most relevant of which arises from precision measurements of the W and Z decays.

a. W and Z decays In order to further probe the parameter space, we perform a simple recast of the result from the ATLAS Collaboration [78] on $pp \to \ell\ell\ell\ell$ (referred to as the $Z \to 4\mu$ search hereafter) in the Z-boson mass window. We implement our effective Lagrangian via FeynRules/UFO [79–81] files, then generate hadron-level events $pp \to \mu\mu\mu\mu$ within the MadGraph5_aMC@NLO platform [82], including the selection cuts from Ref. [78].[4] Our simple simulation chain leads to a SM fiducial cross-section of 22 fb, in good agreement with the predicted SM result from Ref. [78], 21.2 ± 1.3 fb. We therefore use the final measured result of 22.1 ± 1.3 fb to constrain our parameter space. Note that interference with the SM plays an important role in the final cross-section computation.[5] When the FIP is produced on-shell, its couplings to muons can be probed by precision measurements of Drell-Yan dimuon production as was shown in Ref. [84]. We found, however, that this limit is of the same order as the ATLAS bound, or even subdominant, for the mass range $m_V = 1 - 5\,\text{GeV}$ in which it was quoted. Note that the on-shell V production $Z \to \mu\mu V$ participates directly in the $Z \to 4\mu$ search described above and introduces a dependence of this limit to the invisible decay width of V.

In the lower mass regime, the presence of the massive vector FIP longitudinal mode leads to a E^2/m_V^2 enhancement of various SM decay widths. In particular, in the limit $M_\mu, m_V \ll M_Z, M_W$ we find

$$\Gamma(W \to \nu\mu V) \simeq \frac{\left(C_4^{\mu\mu V} - \tilde{C}_4^{\mu\mu V}\right)^2 G_F M_W^5}{512\sqrt{2}\pi^3 m_V^2}\,, \tag{32}$$

and

$$\frac{\Gamma(W \to \nu\mu) + \Gamma(W \to \nu\mu V)}{\Gamma(W \to \nu e)} \simeq 1 + \frac{\Gamma(W \to \nu\mu V)}{\text{BR}_{W\to e\nu}\Gamma_W}\,. \tag{33}$$

We then use the world experimental average on the ratio $\Gamma(W \to \nu\mu)/\Gamma(W \to \nu e)$, 0.996 ± 0.008 [85], to derive the $2\,\sigma$ limit

$$\left|C_4^{\mu\mu V} - \tilde{C}_4^{\mu\mu V}\right| \leq 0.004 \left(\frac{m_V}{100\,\text{MeV}}\right)\,, \tag{34}$$

which holds has long as V decays mostly invisibly. A more conservative limit (which would also apply in presence of electron couplings) is simply to require Eq. (32) to be smaller than the total uncertainty on the measured W width. Using $\Gamma_W = 2.085 \pm 0.042\,\text{GeV}$ from Ref. [85], one obtains the $2\,\sigma$ bound

$$\left|C_4^{\mu\mu V} - \tilde{C}_4^{\mu\mu V}\right| < 0.022 \left(\frac{m_V}{100\,\text{MeV}}\right)\,, \tag{35}$$

which reproduces the result from Ref. [86].

b. Resonance search in B-factories The BaBar Collaboration has searched for the process $e^+e^- \to \mu^+\mu^- V$, $V \to \mu^+\mu^-$, when the FIP is assumed to have a small width and a mass up to around 10 GeV [87]. In the relevant mass region, our model requires in any case a large invisible width to escape resonant $B \to K^*\mu\mu$ searches, so that this constraint is subdominant. The Belle-II Collaboration recently provided a bound on the final-state radiation process $e^+e^- \to \mu^+\mu V$, $V \to$ invisible, based on $0.28\,\text{fb}^{-1}$ of data from the 2018 run [88]. While the current limit can hardly compete with other bounds the 2019 run has stored $\sim 10\,\text{fb}^{-1}$ of data so that the search is expected to become rapidly relevant in the near future.

c. Coupling to electrons We choose not to consider in this work explicit interactions of the FIP with electrons. Nevertheless, a coupling to electrons is generated via the vector kinetic mixing when at least one of the DEFT operators is at dimension 4 [89]. Thus, even below the di-muon threshold, we expect V to decay visibly into e^+e^- in the absence of an invisible decay channel. Constraints on a light vector FIP coupled to electrons were discussed, e.g., in Refs. [4, 5]. In particular, resonance searches at low q^2 in LHCb [12, 90] exclude the parameter space relevant for the $b \to s$ anomalies, thus requiring the V to decay mostly invisibly (in which case the constraints on $B \to K+\text{inv.}$ described above apply).[6]

[3] First results from a similar Belle-II search [77] agree with Refs. [75, 76].

[4] We include the following cuts: four-leptons invariant mass in the range $60 - 100$ GeV, opposite-sign dilepton pair invariant mass larger than 5 GeV, $p_T > 20\,\text{GeV}$ for the leading lepton and $p_T > 10\,\text{GeV}$ for the sub-leading lepton, and an angular separation cut as detailed in Ref. [78].

[5] A somehow similar search was performed by the CMS Collaboration [83] with focus on $L_\mu - L_\tau$ models. It yields constraints similar to the included ATLAS analysis.

[6] LHCb low-resonance searches extend down to $\sim 20\,\text{MeV}$. A very light electron-philic FIP is therefore not constrained by this approach. However, stringent limits on long-lived dark photons then apply, with the parameter space almost completely covered [91].

C. Muon anomalous magnetic moment

If the flavour anomalies are explained by a vector FIP exchange, the same FIP can potentially contribute to the anomalous magnetic moment of the muon. The recent confirmation at Fermilab [34] of a $3.3\,\sigma$ discrepancy between the observed value of $(g-2)_\mu$ and the SM renders this possibility all the more enticing and timely.

The computation of $(g-2)_\mu$ can be enhanced at the 1-loop level if the vector FIP V interacts with the muon current via $\mathcal{Q}_4^{\mu\mu V}$ and $\widetilde{\mathcal{Q}}_4^{\mu\mu V}$. One gets [92, 93]

$$\delta(g-2)_\mu = \frac{1}{8\pi^2}\frac{M_\mu^2}{m_V^2}\left[(\mathcal{C}_4^{\mu\mu V})^2\mathcal{F}(x_\mu) + (\widetilde{\mathcal{C}}_4^{\mu\mu V})^2\tilde{\mathcal{F}}(x_\mu)\right], \tag{36}$$

where $x_\mu = M_\mu/m_V$ and the loop functions read

$$\mathcal{F}(x) = \int_0^1 dz\, \frac{2z^2(1-z)}{x^2 z + (1-z)(1-x^2 z)}\,. \tag{37}$$

$$\tilde{\mathcal{F}}(x) = \int_0^1 dz\, \frac{\left[2z(1-z)(z-4) - 4x^2 z^3\right]}{x^2 z + (1-z)(1-x^2 z)}\,. \tag{38}$$

Conversely, no significant enhancement is obtained if the coupling of the FIP to the muon proceeds through the operators $\mathcal{Q}_6^{\mu\mu V}$ and $\widetilde{\mathcal{Q}}_6^{\mu\mu V}$. In those cases the value of $(g-2)_\mu$ is suppressed by the UV cut-off Λ yielding, for example,

$$\delta(g-2)_\mu = \frac{\left(\mathcal{C}_6^{\mu\mu V}\right)^2 M_\mu^2}{12\,\pi^2\Lambda^2}\,, \tag{39}$$

in the case of $\mathcal{Q}_6^{\mu\mu V}$ and a similar expression for $\widetilde{\mathcal{Q}}_6^{\mu\mu V}$. Its exact numerical value depends entirely on the specifics of the UV completion.

As was described in Sec. IV A, the viable range of the DEFT coefficients $\mathcal{C}_4^{bsV}$, $\mathcal{C}_6^{bsV}$, corresponding to the operators of the $b-s$ current, is bounded by the constraints from B_s-mixing and $B \to K^{(*)} X$ searches. As a direct consequence, for many points in the numerical scan the typical values of $\mathcal{C}_4^{\mu\mu V}$ required for a reasonable agreement with the flavour anomalies is very large, leading to a deviation in $\delta(g-2)_\mu$ widely exceeding the measured value. A cancellation with the contribution from the axial-vector coupling $\widetilde{\mathcal{C}}_4^{\mu\mu V}$ is therefore necessary in most situations [2]. For a GeV-scale vector mediator, this occurs for $\widetilde{\mathcal{C}}_4^{\mu\mu V} \approx \pm 0.44\,\mathcal{C}_4^{\mu\mu V}$. Note, however, that including the axial-vector contribution can trigger the bounds from $B_s \to \mu\mu$, also discussed in Sec. IV A, which are particularly strong in the $m_V \ll 1\,\text{GeV}$ range.

V. NUMERICAL RESULTS

In the rest of this work we will consider somehow arbitrarily FIP masses up to 20 GeV, so that $m_V^2/\Lambda_{\text{EW}}^2 \ll 1$. While there is no specific upper bound on the mass of the vector FIP from the constraints listed in the previous section, we also do not include in our simplified models the interactions between V and the electroweak sector. We leave the complete study of the "transitional" regime for larger masses, up to the electroweak scale Λ_{EW}, for future work.

A. Fit to the $b \to s$ anomalies

We perform a multidimensional fit to the $b \to s$ anomalies, including the LFUV ratios R_K, R_{K^*}, and $B \to K^*\mu^+\mu^-$ angular-observable data. We scan over the following free parameters: m_V, Γ_V, $\mathcal{C}_{4,6}^{bsV}$, $\mathcal{C}_{4,6}^{\mu\mu V}$, and $\widetilde{\mathcal{C}}_{4,6}^{\mu\mu V}$. The vector mass m_V, expressed in GeV, is flatly distributed either in the $[0.01, 2]$ range, or in the $[2, 20]$ one. For the V width, Γ_V, also expressed in GeV, we employ a logarithmically-flat prior in the range $[10^{-3}, 1]$. All the absolute values of the DEFT coefficients have a logarithmically-flat distributed prior in the range $[10^{-10}, 1]$. Since the observables included in these fits depend only on the products $\mathcal{C}_i^{bsV}\cdot\mathcal{C}_j^{\mu\mu V}$ and $\mathcal{C}_i^{bsV}\cdot\widetilde{\mathcal{C}}_j^{\mu\mu V}$, but not on the single coefficients, the fit results presented in this subsection are given in terms of DEFT biproducts rather than as a function of individual coefficients.

As was described in detail in Ref. [8], we perform separate fits depending on whether m_V lies above or below 2 GeV. In fact, in order to obtain an adequate fit, one has to require that the product $\mathcal{C}_i^{bsV}\cdot\mathcal{C}_j^{\mu\mu V}$ ($\mathcal{C}_i^{bsV}\cdot\widetilde{\mathcal{C}}_j^{\mu\mu V}$) assumes a different sign in each of these two regions. We note that this leads to a negative (positive) C_9^μ (C_{10}^μ), in agreement with the global WET fits. Following Ref. [8], we refer to these distinct cases as the *high-mass* fit and the *low-mass* fit.

Due to the q^2 dependence of Eqs. (16), (17), it is not possible to refer explicitly to the results of the global WET fits that can be found in the literature. One needs instead to confront the DEFT parameter space directly with the experimental data. In order to do so, we employ the `HEPfit` package [94], performing a Markov Chain Monte Carlo analysis by means of the Bayesian Analysis Toolkit (BAT) [95].

We present in the upper panel of Fig. 1 the results of the fit in the case of DEFT operators of dimension 4 in both the $b-s$ and $\mu-\mu$ currents (we dub this as the *44 model* hereafter). The plots in magenta are relative to the high-mass fit, where $\mathcal{C}_4^{bsV}\cdot\mathcal{C}_4^{\mu\mu V}$ is required to be positive, the plots in green are relative to the low-mass one, where $\mathcal{C}_4^{bsV}\cdot\mathcal{C}_4^{\mu\mu V}$ is required to be negative, and the contours correspond to the smallest regions of 68%, 95%, 99.7% probability. In particular, in Fig. 1 we are showing the marginalised 2-dimensional posterior probability density function (2D pdf) in planes of the vector mass m_V, its width Γ_V, and the products of DEFT coefficients $\mathcal{C}_4^{bsV}\cdot\mathcal{C}_4^{\mu\mu V}$ and $\mathcal{C}_4^{bsV}\cdot\widetilde{\mathcal{C}}_4^{\mu\mu V}$. In accordance with the respective priors, the posterior pdf's for the width and the coefficients are reported in logarithmic scale. The 2D pdf's involving Γ_V are only shown for the low-mass

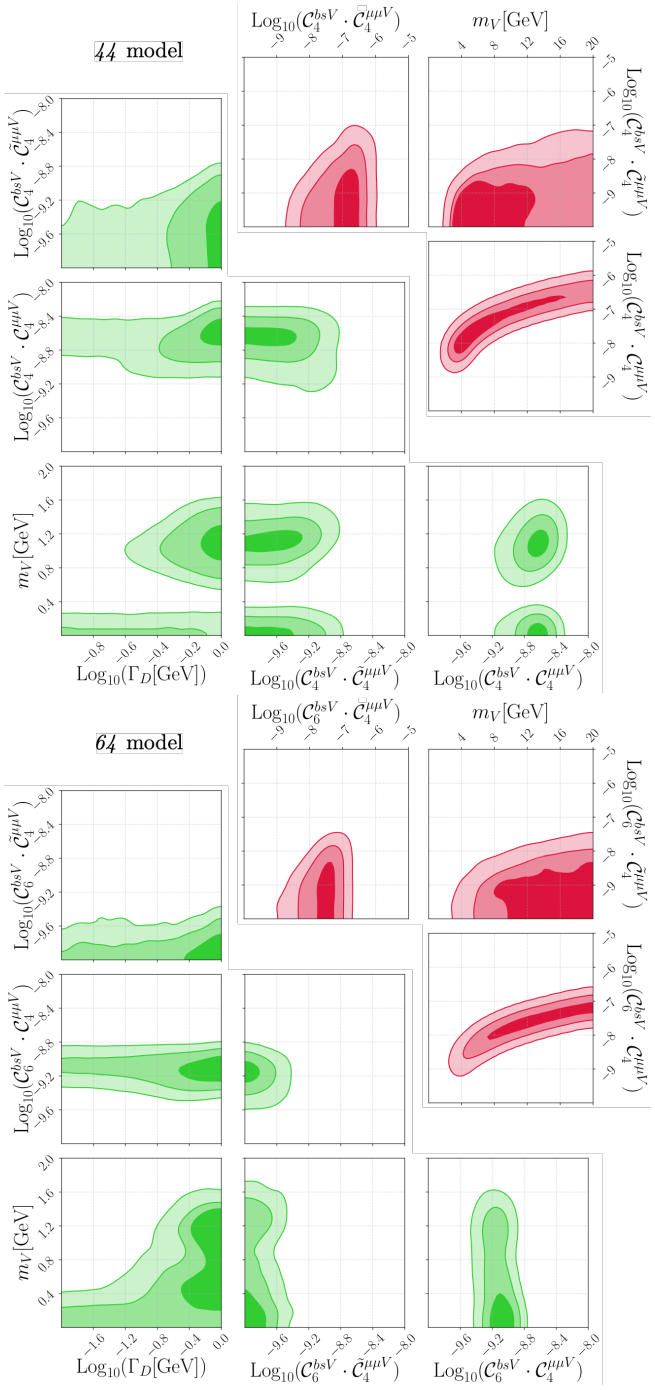

FIG. 1. Inference of model parameters from a fit to $b \to s$ anomalous data. The upper panel refers to DEFT operators of dimension 4 in both the $b-s$ and $\mu-\mu$ currents (*44* model), while the lower panel refers to DEFT operator of dimension 6 in the $b-s$ current and dimension 4 in $\mu-\mu$ (*64* model). The plots in red are relative to the high-mass fits (see main text) while the ones in green are relative to the low-mass ones, with the contours corresponding to the smallest regions of 68%, 95%, 99.7% probability. We refer to the main text for the sign of the couplings. Note that the coupling $\mathcal{C}_6^{bsV}$ is reported in units of GeV^{-2}.

fit since they are flatly distributed and hence not particularly informative in the high-mass case.

In the high-mass region of Fig. 1 (top, magenta) one can observe a strong correlation between the vector mass m_V and the coupling product $\mathcal{C}_4^{bsV}\cdot\mathcal{C}_4^{\mu\mu V}$, responsible for the NP contributions to C_9^μ, cf. Eq. (16). The coupling biproduct can range from $\sim 10^{-8}$ (corresponding to $m_V \approx 4$ GeV) up to $\sim 10^{-6}$ at the $2\,\sigma$ level, if m_V grows as well. From the correlation between $\mathcal{C}_4^{bsV}\cdot\mathcal{C}_4^{\mu\mu V}$ and $\mathcal{C}_4^{bsV}\cdot\tilde{\mathcal{C}}_4^{\mu\mu V}$ it is also possible to observe that the latter can grow from negligible values up to the size of the former (at the $3\,\sigma$ level) but never get larger. This is consistent with the results of global WET fits [22–33], where NP contributions to C_{10}^μ – which, as Eq. (17) shows, in the DEFT arise precisely from $\mathcal{C}_4^{bsV}\cdot\tilde{\mathcal{C}}_4^{\mu\mu V}$ – are, if non-vanishing, usually smaller in size than the ones to C_9^μ.[7]

In the low-mass region $\mathcal{C}_4^{bsV}\cdot\mathcal{C}_4^{\mu\mu V}$ is constrained to about $10^{-9.0} - 10^{-8.4}$, in correspondence of which m_V can assume two distinct values, one peaked around 1 GeV and the other around 50 MeV. While the origin of these disconnected solutions is not evident, it can be tracked back to the peculiar q^2 dependence of Eq. (16), which can give rise, for specific choices of m_V, to destructive and/or constructive interference in the WET Wilson coefficients that are fitted to the experimental bins. Note that the solution with $m_V \approx 1\,\mathrm{GeV}$ requires a large width, as highlighted by the peak around $\Gamma_V \approx 1\,\mathrm{GeV}$ in the posterior pdf. This does not seem to be the case instead for $m_V \approx 50\,\mathrm{MeV}$. Finally, analogous to what happens in the high-mass fit, the biproduct $\mathcal{C}_4^{bsV}\cdot\tilde{\mathcal{C}}_4^{\mu\mu V}$ is found to be smaller than $\mathcal{C}_4^{bsV}\cdot\mathcal{C}_4^{\mu\mu V}$.

The fit results in the case of DEFT operators of dimension 6 in the $b-s$ current and dimension 4 in $\mu-\mu$ are presented in the lower panel of Fig. 1 (we dub this as the *64 model* hereafter). The colour scheme is the same as for the top panel. $\mathcal{C}_6^{bsV}\cdot\mathcal{C}_4^{\mu\mu V}$ is required to be negative in the high-mass region, and positive in the low-mass one. While quantitative differences with respect to the *44* model can be found in this case, driven by the different q^2 dependence of the NP contributions, we can also highlight a few qualitative similarities. One pertains to the correlation between m_V and the coupling product $\mathcal{C}_6^{bsV}\cdot\mathcal{C}_4^{\mu\mu V}$ in the high-mass region, which is similar to the corresponding correlation in the top panel. However, the high-probability region of the pdf is peaked now at higher m_V. Another similarity emerges in the low-mass region, where $\mathcal{C}_6^{bsV}\cdot\mathcal{C}_4^{\mu\mu V}$ is again bound to a

[7] Exceptions to this statement apply if one advocates for a very conservative treatment of the hadronic uncertainties or, alternatively, for an additional universal NP component in both the electron and muon vector currents. Indeed, if one allows for either one of these possibilities it becomes easier to accommodate NP contributions to the muon axial current of the same size as the ones in the muon vector current (and hence $|\mathcal{C}_4^{\mu\mu V}| \approx |\tilde{\mathcal{C}}_4^{\mu\mu V}|$) [23, 24, 27, 29, 31, 33].

very narrow range. Note, however, that the two separate m_V ranges found in the *44* model have now merged into one single high-probability region. All values up to $m_V \approx 1.4$ GeV are allowed at the $2\,\sigma$ level. Nevertheless, while for $m_V \approx 1\,\text{GeV}$ a large Γ_V is needed to fit the LFUV anomalies correctly, this is not the case for $m_V \lesssim 200\,\text{MeV}$, in similar fashion to the *44* model.

As a final remark, we point out that a fit performed in the case of DEFT operators of dimension 4 in the $b-s$ current and dimension 6 in $\mu-\mu$ (*46 model*) yields results perfectly analogous to the ones shown in the lower panel of Fig. 1, given the equal q^2 dependence of the two scenarios, presented in Eqs. (16), (17). On the other hand, the results of a fit where the couplings to the $b-s$ and $\mu-\mu$ currents arise both from DEFT operators of dimension 6 (*66 model*) can be found in Appendix A.

B. Including all flavour constraints

We can now apply the constraints introduced in Sec. IV A-IV B to the high-probability regions of the fits described above. We present the results in Fig. 2, in the plane of the vector muon coupling versus the FIP mass m_V. The yellow points in the figure are within the $2\,\sigma$ regions of the fits to $b \to s$ anomalies described in Sec. V A. Green points satisfy, additionally, the $B \to K$+inv., $B \to K^* \mu\mu$, $B_s - \bar{B}_s$ mixing, $B_s \to \mu\mu$ constraints and $Z \to \mu\mu V$ in ATLAS at the $2\,\sigma$ level. Since some of the constraints on the muon coupling depend on the invisible decay width of the FIP, we also apply to each green point the "invisible" constraints from the BaBar searches [75, 76], numerically recast as described in Ref. [8]. We finally overlay the remaining limits, which are independent of $\Gamma_{V,\text{inv}}$. The green band corresponds to $\mathcal{C}_4^{\mu\mu V}$ being consistent at $2\,\sigma$ with the $(g-2)_\mu$ measurement [34]. Some of the constraints applied to the parameter space depend explicitly on both $\mathcal{C}_4^{\mu\mu V}$ and $\widetilde{\mathcal{C}}_4^{\mu\mu V}$. This is the case particularly for the W-decay bound of Eq. (32) and forward, and for the numerical recast of the $Z \to 4\mu$ cross-section bound. When these bounds are applied to regions of the parameter space for which $\mathcal{C}_4^{\mu\mu V}$ is too large to yield a value of $\delta(g-2)_\mu$ in agreement with the experimental determination, we tune $\widetilde{\mathcal{C}}_4^{\mu\mu V}$ as required to bring $\delta(g-2)_\mu$ down to the measured $2\,\sigma$ region, cf. Sec. IV C.[8]

FIPs with mass above the B-meson can easily yield an excellent fit to the experimental data while escaping all current constraints. This is in agreement with the results obtained in the UV model of Ref. [8]. This conclusion holds for the *44* model, shown in the top panel of Fig. 2, as well as for the *64* model, shown in the bottom panel. Incidentally, we find it remarkable that these very compact simplified-model solutions to the $b \to s$ anomalies feature also excellent prospect to solve the $(g-2)_\mu$ anomaly. In this region, the lower limit on the green points distribution arises from the B_s-mixing constraints on $\mathcal{C}_4^{bsV}$ and $\mathcal{C}_6^{bsV}$ and the upper limit from the ATLAS Collaboration [78] search for $Z \to 4\mu$ search.

We observe that in the *64* model the fit yields a large number of points compatible with the various B-physics constraints in the very low-mass region of the parameter space, $m_V \ll 2\,M_\mu$. On the other hand, the required couplings to the muon are typically quite large, to overcome the strong bounds on $\mathcal{C}_6^{bsV}/\Lambda^2$ from $B \to K +$ invisible. This leads to $\delta(g-2)_\mu$ exceeding the experimental value and, consequently, a unified solution to all anomalies requires the aforementioned fine tuning of the axial-vector muon coupling against the vector one. The overwhelming majority of these points are excluded by flavour-universality tests in W decays, as measured at the LHC [85].

We point out, finally, that in the presence of a neutrino coupling, stringent constraints from neutrino trident production apply [56], potentially excluding a common solution for the $(g-2)_\mu$ and LFUV anomalies in the high-mass region. For indicative purposes we show as a dotted purple line in both panels of Fig. 2 the upper bound obtained under the assumption that the coupling of V to neutrinos is of the same size as $\mathcal{C}_4^{\mu\mu V}$. This would be indeed the case for $\text{SU}(2)_L$-conserving interactions of the V with the lepton doublet, like in the well-known $L_\mu - L_\tau$ gauge group. However, it is not difficult to envision more elaborate UV constructions that could allow one to suppress the coupling to the neutrino with respect to the corresponding charged lepton, in which case the purple line in Fig. 2 would shift upwards.

VI. SUMMARY AND CONCLUSIONS

In this paper we have performed a comprehensive phenomenological analysis of a set of simplified models providing a combined solution to the anomalous magnetic moment of the muon and the flavour anomalies emerged at LHCb in $b \to s l^+ l^-$ transitions (both flavour-conserving and lepton-flavour violating). Our simplified models are based on a set of operators of the Dark EFT, or DEFT, where with this term we encompass a broad range of interactions between the SM and one or more light, feebly interacting particles, or FIPs. We find that the most promising models for fitting both anomalies are based on vector FIPs, with the FIP exchange at low energy giving rise to the anomalies in flavour and $(g-2)_\mu$.

We have further divided our simplified models in categories determined by the explicit momentum dependence of the FIP interaction with the $b-s$ and $\mu-\mu$ vector currents. For all categories, after performing a global fit to the experimental data we have applied a large set of con-

[8] As the sign of $\widetilde{\mathcal{C}}_4^{\mu\mu V}$ is not fixed by this procedure, we choose it in agreement with the requirements from the $b \to s$ fits, i.e., opposite to the sign of $\mathcal{C}_4^{\mu\mu V}$.

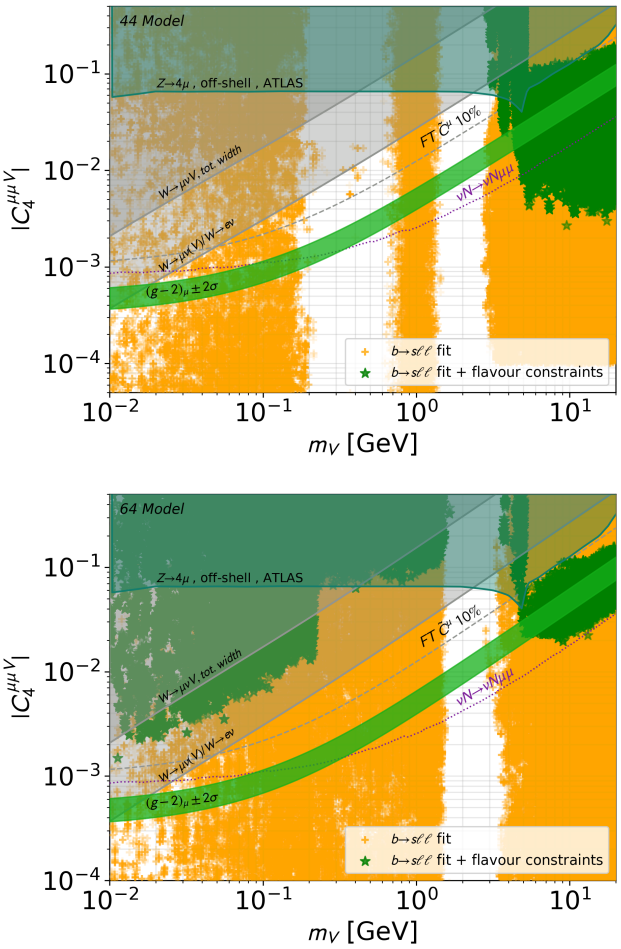

FIG. 2. Constraints on the parameter space consistent with the LFUV anomalies (yellow points) in the plane of $\mathcal{C}_4^{\mu\mu V}$ versus the vector mass m_V. The *44* model is shown in the top panel and the *64* model in the bottom one. Besides being consistent at $2\,\sigma$ with the $b \to s$ anomalies, all green points satisfy the constraints from $B \to K+\text{inv.}$, $B \to K^*\mu\mu$, $B_s - \bar{B}_s$ mixing and $B_s \to \mu\mu$ at 2σ, applied following the procedure described in the text. We show overlaid the bounds that do not depend on the hadronic sector. The blue region covers the parameter space excluded by the multilepton ATLAS search [78], whereas the grey regions show bounds from LFUV in W-decay (see main text). The green band is consistent with the $(g-2)_\mu$ measurement [34] at $2\,\sigma$, with no fine tuning of the couplings. All points above the green band require a non-zero $\widetilde{\mathcal{C}}_4^{\mu\mu V}$, with the dashed grey line indicating a 10% fine tuning with $\mathcal{C}_4^{\mu\mu V}$. The dotted purple line in both panels shows the upper bound from neutrino trident production [56], obtained under the assumption that the coupling of V to neutrinos is of the same size as $\mathcal{C}_4^{\mu\mu V}$.

straints to the favoured parameter space, extracted from direct measurements of the $B \to K + \text{invisible}$ branching ratio, $B \to K^*\mu^+\mu^-$ resonant decays, the measurements of $\text{BR}(B_s \to \mu^+\mu^-)$, B_s-mixing and several precision measurements associated with the W and Z boson decay widths.

We find that unified explanations of the $(g-2)_\mu$ and $b \to sl^+l^-$ anomalies exist and pass all the constraints in a model based on vector-mediator exchange with DEFT operators of dimension 4 in both the $b-s$ and $\mu-\mu$ vector currents (model *44*, with no momentum-dependence of the couplings), and in vector-mediator exchange with dimension 6 in the $b-s$ current (q^2-dependence of the coupling) and dimension 4 in $\mu-\mu$ (we call it model *64*). In both models the typical range of the vector mediator mass is $m_V \gtrsim 4\,\text{GeV}$ and the solution to the $(g-2)_\mu$ anomaly does not require any fine tuning of the vector and axial-vector couplings of the V with the muon. We have found additionally that the observables $B_s \to \mu\mu$ and ΔM_{B_s} will be able to discriminate between models *44* and *64* in this mass range. FIPs with $m_V > 20\,\text{GeV}$ are also likely to provide a good fit to the $b \to sl^+l^-$ anomalies. However, we have worked here under the assumption that the mixing of V with the electroweak sector of the SM can be neglected. As this hypothesis may break down when approaching closely the Z mass from below, possibly leading to additional limits from processes such as $Z \to \gamma V$ and others, we leave a proper study of the "transitional" regime between light and heavy NP to future work.

While in model *44* the only viable unified solution lies in the $m_V \gtrsim 4\,\text{GeV}$ range, in model *64* the global analysis to $b \to sl^+l^-$ additionally highlights a region of good fit at $m_V \approx 0.01 - 1\,\text{GeV}$ passing all flavour constraints. However, this region of the parameter space is characterised by a large muon coupling and requires large fine tuning of the vector and axial-vector contributions to satisfy the $\delta(g-2)_\mu$ measurement. More importantly, we find that an upper bound on the muon coupling imposed by the $\Gamma(W \to \mu\nu V)$ measured width entirely excludes this region of the parameter space.

In summary, we have highlighted in this work viable solutions for a combined explanation of the $(g-2)_\mu$ and $b \to sl^+l^-$ anomalies, based on the simple exchange of a light particle and characterised by a very minimal set of assumptions. Our goal is that of providing a self-standing and fairly broad compendium of the low-energy experimental bounds affecting these scenarios. The emerging parameter space regions and coupling strengths can then be used at face value to guide the model-building efforts in the high-energy sector.

ACKNOWLEDGMENTS

L.D. is supported by the INFN "Iniziativa Specifica" Theoretical Astroparticle Physics (TAsP-LNF). The work of M.F. is supported by the Deutsche Forschungsgemeinschaft (DFG, German Research Foundation) under grant 396021762 - TRR 257, "Particle Physics Phenomenology after the Higgs Discovery". K.K. is partially supported by the National Science Centre (Poland) under the research Grant

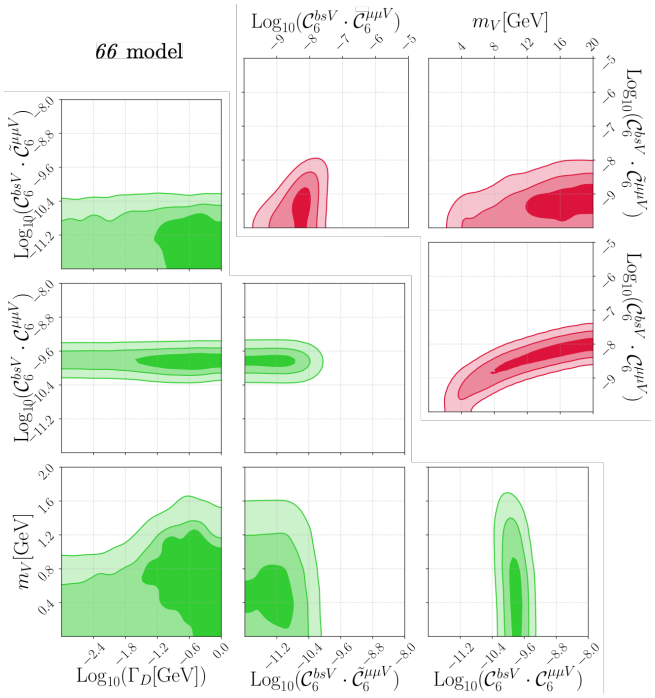

FIG. 3. Inference of model parameters from a fit to $b \to s$ anomalous data with DEFT operators of dimension 6 in both the $b-s$ and $\mu-\mu$ currents (*66* model). The colour scheme is the same as in Fig. 1. Note that the couplings $\mathcal{C}_6^{bsV}$, $\mathcal{C}_6^{\mu\mu V}$ and $\tilde{\mathcal{C}}_6^{\mu\mu V}$ are reported in units of GeV^{-2}.

No. 2017/26/E/ST2/00470. E.M.S. is supported in part by the National Science Centre (Poland) under the research Grant No. 2017/26/D/ST2/00490.

Appendix A: 66 model

We present in Fig. 3 the marginalised 2D pdf of the fit in the case of DEFT operators of dimension 6 in both the $b-s$ and $\mu-\mu$ currents (*66 model*). The colour scheme is the same as in Fig. 1. The fit shows many qualitative similarities to the *64* case, with the main differences pertaining mostly to the favoured values of the couplings due to the different q^2 dependence.

We show in Fig. 4 the corresponding result once all the flavour constraints have been applied. There appear to be extremely few points that can pass all the cuts simultaneously, with the limit from the multilepton ATLAS search [78] dominating the constraints on the muon coupling. This exclusion reflects the fact that the FIP coupling to the muon, $\mathcal{C}_6^{\mu\mu V}$, is of dimension 6 and thus more sensitive to high-energy processes then in the *44* and *64* cases.

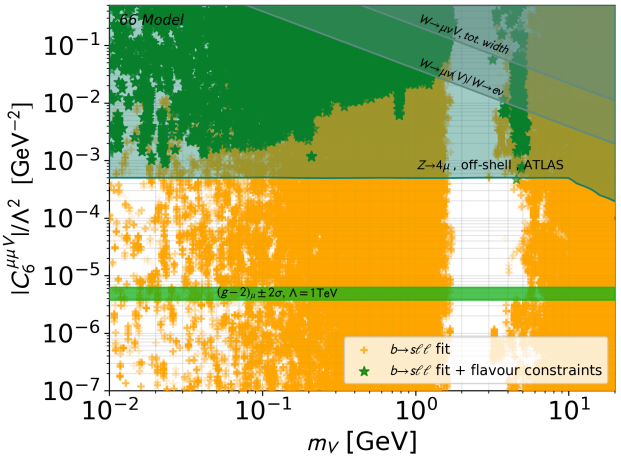

FIG. 4. Constraints on the parameter space consistent with the LFUV anomalies (yellow points) in the plane of $\mathcal{C}_6^{\mu\mu V}$ versus the vector mass m_V for the *66* model. The colour scheme is the same as in Fig. 2. The position of the $(g-2)_\mu$ $2\,\sigma$ band corresponds to a UV scale $\Lambda = 1\,\mathrm{TeV}$.

[1] A. Datta, J. Liao, and D. Marfatia, Phys. Lett. **B768**, 265 (2017), arXiv:1702.01099 [hep-ph].
[2] F. Sala and D. M. Straub, Phys. Lett. **B774**, 205 (2017), arXiv:1704.06188 [hep-ph].
[3] A. K. Alok, B. Bhattacharya, A. Datta, D. Kumar, J. Kumar, and D. London, Phys. Rev. **D96**, 095009 (2017), arXiv:1704.07397 [hep-ph].
[4] A. Datta, J. Kumar, J. Liao, and D. Marfatia, Phys. Rev. **D97**, 115038 (2018), arXiv:1705.08423 [hep-ph].
[5] W. Altmannshofer, M. J. Baker, S. Gori, R. Harnik, M. Pospelov, E. Stamou, and A. Thamm, JHEP **03**, 188 (2018), arXiv:1711.07494 [hep-ph].
[6] A. Datta, B. Dutta, S. Liao, D. Marfatia, and L. E. Strigari, JHEP **01**, 091 (2019), arXiv:1808.02611 [hep-ph].
[7] A. Datta, J. L. Feng, S. Kamali, and J. Kumar, Phys. Rev. **D101**, 035010 (2020), arXiv:1908.08625 [hep-ph].
[8] L. Darmé, M. Fedele, K. Kowalska, and E. M. Sessolo, JHEP **08**, 148 (2020), arXiv:2002.11150 [hep-ph].
[9] R. Aaij *et al.* (LHCb), (2021), arXiv:2103.11769 [hep-ex].
[10] R. Aaij *et al.* (LHCb), JHEP **08**, 055 (2017), arXiv:1705.05802 [hep-ex].
[11] A. Abdesselam *et al.* (Belle), (2019), arXiv:1904.02440 [hep-ex].
[12] R. Aaij *et al.* (LHCb), JHEP **04**, 064 (2015), arXiv:1501.03038 [hep-ex].
[13] R. Aaij *et al.* (LHCb), JHEP **09**, 179 (2015), arXiv:1506.08777 [hep-ex].
[14] V. Khachatryan *et al.* (CMS), Phys. Lett. B **753**, 424 (2016), arXiv:1507.08126 [hep-ex].

[15] R. Aaij *et al.* (LHCb), JHEP **02**, 104 (2016), arXiv:1512.04442 [hep-ex].
[16] R. Aaij *et al.* (LHCb), JHEP **11**, 047 (2016), [Erratum: JHEP04,142(2017)], arXiv:1606.04731 [hep-ex].
[17] S. Wehle *et al.* (Belle), Phys. Rev. Lett. **118**, 111801 (2017), arXiv:1612.05014 [hep-ex].
[18] A. M. Sirunyan *et al.* (CMS), Phys. Lett. **B781**, 517 (2018), arXiv:1710.02846 [hep-ex].
[19] M. Aaboud *et al.* (ATLAS), JHEP **10**, 047 (2018), arXiv:1805.04000 [hep-ex].
[20] R. Aaij *et al.* (LHCb), Phys. Rev. Lett. **125**, 011802 (2020), arXiv:2003.04831 [hep-ex].
[21] R. Aaij *et al.* (LHCb), Phys. Rev. Lett. **126**, 161802 (2021), arXiv:2012.13241 [hep-ex].
[22] G. D'Amico, M. Nardecchia, P. Panci, F. Sannino, A. Strumia, R. Torre, and A. Urbano, JHEP **09**, 010 (2017), arXiv:1704.05438 [hep-ph].
[23] M. Ciuchini, A. M. Coutinho, M. Fedele, E. Franco, A. Paul, L. Silvestrini, and M. Valli, Eur. Phys. J. **C79**, 719 (2019), arXiv:1903.09632 [hep-ph].
[24] M. Algueró, B. Capdevila, A. Crivellin, S. Descotes-Genon, P. Masjuan, J. Matias, and J. Virto, Eur. Phys. J. **C79**, 714 (2019), arXiv:1903.09578 [hep-ph].
[25] A. K. Alok, A. Dighe, S. Gangal, and D. Kumar, JHEP **06**, 089 (2019), arXiv:1903.09617 [hep-ph].
[26] A. Datta, J. Kumar, and D. London, Phys. Lett. **B797**, 134858 (2019), arXiv:1903.10086 [hep-ph].
[27] J. Aebischer, W. Altmannshofer, D. Guadagnoli, M. Reboud, P. Stangl, and D. M. Straub, (2019), arXiv:1903.10434 [hep-ph].
[28] K. Kowalska, D. Kumar, and E. M. Sessolo, Eur. Phys. J. **C79**, 840 (2019), arXiv:1903.10932 [hep-ph].
[29] M. Ciuchini, M. Fedele, E. Franco, A. Paul, L. Silvestrini, and M. Valli, Phys. Rev. D **103**, 015030 (2021), arXiv:2011.01212 [hep-ph].
[30] T. Hurth, F. Mahmoudi, and S. Neshatpour, (2020), arXiv:2012.12207 [hep-ph].
[31] W. Altmannshofer and P. Stangl, (2021), arXiv:2103.13370 [hep-ph].
[32] L.-S. Geng, B. Grinstein, S. Jäger, S.-Y. Li, J. Martin Camalich, and R.-X. Shi, (2021), arXiv:2103.12738 [hep-ph].
[33] M. Algueró, B. Capdevila, S. Descotes-Genon, J. Matias, and M. Novoa-Brunet, in *55th Rencontres de Moriond on QCD and High Energy Interactions* (2021) arXiv:2104.08921 [hep-ph].
[34] B. Abi *et al.* (Muon $g-2$ Collaboration), Phys. Rev. Lett. **126**, 141801 (2021).
[35] M. Davier, A. Hoecker, B. Malaescu, and Z. Zhang, Eur. Phys. J. C **77**, 827 (2017), arXiv:1706.09436 [hep-ph].
[36] A. Keshavarzi, D. Nomura, and T. Teubner, Phys. Rev. D **97**, 114025 (2018), arXiv:1802.02995 [hep-ph].
[37] G. Colangelo, M. Hoferichter, and P. Stoffer, JHEP **02**, 006 (2019), arXiv:1810.00007 [hep-ph].
[38] M. Hoferichter, B.-L. Hoid, and B. Kubis, JHEP **08**, 137 (2019), arXiv:1907.01556 [hep-ph].
[39] M. Davier, A. Hoecker, B. Malaescu, and Z. Zhang, Eur. Phys. J. C **80**, 241 (2020), [Erratum: Eur.Phys.J.C 80, 410 (2020)], arXiv:1908.00921 [hep-ph].
[40] A. Keshavarzi, D. Nomura, and T. Teubner, Phys. Rev. D **101**, 014029 (2020), arXiv:1911.00367 [hep-ph].
[41] A. Kurz, T. Liu, P. Marquard, and M. Steinhauser, Phys. Lett. B **734**, 144 (2014), arXiv:1403.6400 [hep-ph].
[42] K. Melnikov and A. Vainshtein, Phys. Rev. D **70**, 113006 (2004), arXiv:hep-ph/0312226.
[43] P. Masjuan and P. Sanchez-Puertas, Phys. Rev. D **95**, 054026 (2017), arXiv:1701.05829 [hep-ph].
[44] G. Colangelo, M. Hoferichter, M. Procura, and P. Stoffer, JHEP **04**, 161 (2017), arXiv:1702.07347 [hep-ph].
[45] M. Hoferichter, B.-L. Hoid, B. Kubis, S. Leupold, and S. P. Schneider, JHEP **10**, 141 (2018), arXiv:1808.04823 [hep-ph].
[46] A. Gérardin, H. B. Meyer, and A. Nyffeler, Phys. Rev. D **100**, 034520 (2019), arXiv:1903.09471 [hep-lat].
[47] J. Bijnens, N. Hermansson-Truedsson, and A. Rodríguez-Sánchez, Phys. Lett. B **798**, 134994 (2019), arXiv:1908.03331 [hep-ph].
[48] G. Colangelo, F. Hagelstein, M. Hoferichter, L. Laub, and P. Stoffer, JHEP **03**, 101 (2020), arXiv:1910.13432 [hep-ph].
[49] G. Colangelo, M. Hoferichter, A. Nyffeler, M. Passera, and P. Stoffer, Phys. Lett. B **735**, 90 (2014), arXiv:1403.7512 [hep-ph].
[50] T. Blum, N. Christ, M. Hayakawa, T. Izubuchi, L. Jin, C. Jung, and C. Lehner, Phys. Rev. Lett. **124**, 132002 (2020), arXiv:1911.08123 [hep-lat].
[51] T. Aoyama, M. Hayakawa, T. Kinoshita, and M. Nio, Phys. Rev. Lett. **109**, 111808 (2012), arXiv:1205.5370 [hep-ph].
[52] T. Aoyama, T. Kinoshita, and M. Nio, Atoms **7** (2019), 10.3390/atoms7010028.
[53] A. Czarnecki, W. J. Marciano, and A. Vainshtein, Phys. Rev. D **67**, 073006 (2003), [Erratum: Phys.Rev.D 73, 119901 (2006)], arXiv:hep-ph/0212229.
[54] C. Gnendiger, D. Stöckinger, and H. Stöckinger-Kim, Phys. Rev. D **88**, 053005 (2013), arXiv:1306.5546 [hep-ph].
[55] G. W. Bennett *et al.* (Muon g-2), Phys. Rev. **D73**, 072003 (2006), arXiv:hep-ex/0602035 [hep-ex].
[56] W. Altmannshofer, S. Gori, M. Pospelov, and I. Yavin, Phys. Rev. Lett. **113**, 091801 (2014), arXiv:1406.2332 [hep-ph].
[57] W. Altmannshofer, P. Stangl, and D. M. Straub, Phys. Rev. **D96**, 055008 (2017), arXiv:1704.05435 [hep-ph].
[58] C. Arina, J. Hajer, and P. Klose, (2021), arXiv:2105.06477 [hep-ph].
[59] P. J. Fox, R. Harnik, J. Kopp, and Y. Tsai, Phys. Rev. D **84**, 014028 (2011), arXiv:1103.0240 [hep-ph].
[60] M. Duch, B. Grzadkowski, and J. Wudka, JHEP **05**, 116 (2015), arXiv:1412.0520 [hep-ph].
[61] F. Bishara, J. Brod, B. Grinstein, and J. Zupan, JCAP **02**, 009 (2017), arXiv:1611.00368 [hep-ph].
[62] A. De Simone and T. Jacques, Eur. Phys. J. C **76**, 367 (2016), arXiv:1603.08002 [hep-ph].
[63] L. Darmé, S. A. R. Ellis, and T. You, JHEP **07**, 053 (2020), arXiv:2001.01490 [hep-ph].
[64] P. J. Fox, I. Low, and Y. Zhang, JHEP **03**, 074 (2018), arXiv:1801.03505 [hep-ph].
[65] P. Arnan, A. Crivellin, M. Fedele, and F. Mescia, JHEP **06**, 118 (2019), arXiv:1904.05890 [hep-ph].
[66] J. Gracey, Phys. Lett. B **488**, 175 (2000), arXiv:hep-ph/0007171.
[67] J. A. Dror, R. Lasenby, and M. Pospelov, Phys. Rev. D **96**, 075036 (2017), arXiv:1707.01503 [hep-ph].
[68] J. A. Dror, R. Lasenby, and M. Pospelov, Phys. Rev. Lett. **119**, 141803 (2017), arXiv:1705.06726 [hep-ph].
[69] L. Michaels and F. Yu, JHEP **03**, 120 (2021), arXiv:2010.00021 [hep-ph].

[70] *Combination of the ATLAS, CMS and LHCb results on the $B^0_{(s)} \to \mu^+\mu^-$ decays.*, Tech. Rep. (CERN, Geneva, 2020) all figures including auxiliary figures are available at https://atlas.web.cern.ch/Atlas/GROUPS/PHYSICS/CONFNOTES/ATLAS-CONF-2020-049.

[71] M. Beneke, C. Bobeth, and R. Szafron, JHEP **10**, 232 (2019), arXiv:1908.07011 [hep-ph].

[72] P. A. Zyla *et al.* (Particle Data Group), Prog. Theor. Exp. Phys. , 083C01 (2020).

[73] S. Aoki *et al.* (Flavour Lattice Averaging Group), Eur. Phys. J. C **80**, 113 (2020), arXiv:1902.08191 [hep-lat].

[74] R. Aaij *et al.* (LHCb), Phys. Rev. Lett. **115**, 161802 (2015), arXiv:1508.04094 [hep-ex].

[75] P. del Amo Sanchez *et al.* (BaBar), Phys. Rev. **D82**, 112002 (2010), arXiv:1009.1529 [hep-ex].

[76] J. P. Lees *et al.* (BaBar), Phys. Rev. **D87**, 112005 (2013), arXiv:1303.7465 [hep-ex].

[77] F. Abudinén *et al.* (Belle-II), (2021), arXiv:2104.12624 [hep-ex].

[78] G. Aad *et al.* (ATLAS), (2021), arXiv:2103.01918 [hep-ex].

[79] N. D. Christensen, P. de Aquino, C. Degrande, C. Duhr, B. Fuks, M. Herquet, F. Maltoni, and S. Schumann, Eur. Phys. J. C **71**, 1541 (2011), arXiv:0906.2474 [hep-ph].

[80] C. Degrande, C. Duhr, B. Fuks, D. Grellscheid, O. Mattelaer, and T. Reiter, Comput. Phys. Commun. **183**, 1201 (2012), arXiv:1108.2040 [hep-ph].

[81] A. Alloul, N. D. Christensen, C. Degrande, C. Duhr, and B. Fuks, Comput. Phys. Commun. **185**, 2250 (2014), arXiv:1310.1921 [hep-ph].

[82] J. Alwall, R. Frederix, S. Frixione, V. Hirschi, F. Maltoni, O. Mattelaer, H. S. Shao, T. Stelzer, P. Torrielli, and M. Zaro, JHEP **07**, 079 (2014), arXiv:1405.0301 [hep-ph].

[83] A. M. Sirunyan *et al.* (CMS), Phys. Lett. B **792**, 345 (2019), arXiv:1808.03684 [hep-ex].

[84] F. Bishara, U. Haisch, and P. F. Monni, Phys. Rev. **D96**, 055002 (2017), arXiv:1705.03465 [hep-ph].

[85] P. A. Zyla *et al.* (Particle Data Group), PTEP **2020**, 083C01 (2020).

[86] S. G. Karshenboim, D. McKeen, and M. Pospelov, Phys. Rev. D **90**, 073004 (2014), [Addendum: Phys.Rev.D 90, 079905 (2014)], arXiv:1401.6154 [hep-ph].

[87] J. P. Lees *et al.* (BaBar), Phys. Rev. D **94**, 011102 (2016), arXiv:1606.03501 [hep-ex].

[88] I. Adachi *et al.* (Belle-II), (2019), arXiv:1912.11276 [hep-ex].

[89] B. Holdom, Phys. Lett. B **166**, 196 (1986).

[90] R. Aaij *et al.* (LHCb), JHEP **05**, 159 (2013), arXiv:1304.3035 [hep-ex].

[91] J. Beacham *et al.*, J. Phys. **G47**, 010501 (2020), arXiv:1901.09966 [hep-ex].

[92] F. Jegerlehner and A. Nyffeler, Phys. Rept. **477**, 1 (2009), arXiv:0902.3360 [hep-ph].

[93] F. S. Queiroz and W. Shepherd, Phys. Rev. **D89**, 095024 (2014), arXiv:1403.2309 [hep-ph].

[94] J. De Blas *et al.*, Eur. Phys. J. C **80**, 456 (2020), arXiv:1910.14012 [hep-ph].

[95] A. Caldwell, D. Kollar, and K. Kroninger, Comput. Phys. Commun. **180**, 2197 (2009), arXiv:0808.2552 [physics.data-an].